ISSN 1070-3284, Russian Journal of Coordination Chemistry, 2023, Vol. 49, No. 8, pp. 503–512. © Pleiades Publishing, Ltd., 2023.
Russian Text © The Author(s), 2023, published in Koordinatsionnaya Khimiya, 2023, Vol. 49, No. 8, pp. 493–503.

# Trimethylplatinum(IV) Complexes for MOCVD Applications: A Physicochemical Study

**S. I. Dorovskikh[a], *, N. V. Kuratieva[a], I. V. Korolkov[a], T. V. Basova[a], and I. Yu. Ilyin[a]**

[a] *Nikolaev Institute of Inorganic Chemistry, Siberian Branch, Russian Academy of Sciences, Novosibirsk, Russia*

**e-mail: dorov@niic.nsc.ru*

Received December 28, 2022; revised January 31, 2023; accepted March 3, 2023

**Abstract**—The structure of trimethylplatinum(IV) iodide $[(CH_3)_3PtI]_4$ (**I**) (CIF file CCDC no. 22330007) is refined. The structure of the synthesized for the first time trimethylplatinum(IV) complex with tridentate *N*,*N*,*O*-iminoketonate $[(CH_3)_3Pt(C_9H_{17}N_2O)]$ (**II**) is determined by X-ray diffraction (XRD) (CIF file CCDC no. 22330008). The purity of the isolated phases is confirmed by elemental analysis and IR and NMR spectroscopy. The thermal behavior of complex **II** is studied by thermogravimetry. The energies of ionization and fragmentation of the molecules of complex **II** leading to the formation of the most stable fragment $[(CH_3)_3Pt]^+$ are estimated by quantum-chemical calculations. Complex **II** is tested in the MOCVD processes. The Pt films with the pronounced (111) texture and particle sizes about 100 nm are prepared on Si plates in the presence of oxygen.

**Keywords:** trimethylplatinum(IV) complexes, XRD, thermogravimetry, DFT, MOCVD

**DOI:** 10.1134/S1070328423600353

## INTRODUCTION

Trimethylplatinum(IV) complexes with halogen ligands are important starting substances for the synthesis of a wide series of the trimethylplatinum(IV) compounds demanded in the areas of coordination and structural chemistry [1, 2], in the gas-phase syntheses of the platinum nanomaterials [3, 4], and for the preparation of bimetallic catalysts (2,2-bipyridyl)$PtMe_3X$, where X = $Mn(CO)_5$, $ReO_3$ with Pt–metal bonds [5, 6]. The modern research is focused on the trimethylplatinum(IV) complexes with nitrogen-containing aromatic ligands. For example, their dynamic behavior in solutions and the influence of the solvent type on the activation of C–H bonds were reported [7–9], and the reactivity of the trimethylplatinum(IV) complexes with the diamine and *N*,*N*- and *O*,*N*-carbene ligands in acetone solutions in the intramolecular reduction of platinum with ethane formation was studied [10, 11].

There are a few works on studying transformations of the trimethylplatinum(IV) complexes in the gas phase, and they are mainly devoted to specific features of the decomposition of adsorbed molecules of $[(CH_3)_3PtCp^R]$ ($Cp^R$ = cyclopentadienyl ligands) [12, 13] and $[(CH_3)_3PtLPy]$ (L is β-diketonate ligand, Py is pyridine) [14, 15] for the deposition of platinum nanomaterials from the gas phase named metal-organic chemical vapor deposition (MOCVD). An importance of pyridine application in the synthesis of precursors of the $[(CH_3)_3PtLPy]$ series was substantiated [16, 17], since nonvolatile $[(CH_3)_3PtL]_n$ complexes with the Pt–C bridging bond are formed in the absence of pyridine. The decomposition of $[(CH_3)_3Pt^{IV}Cp^{Me}]$ vapors on the substrate surface bearing OH groups is accompanied by intramolecular rearrangements at the $Pt–CH_3$ bond to form adsorbed $\{(CH_3)_nPt(Cp^{Me})\}$ fragments and methane [18]. On the contrary, on going from $[(CH_3)_3PtCp^R]$ to the $[(CH_3)_3PtLPy]$ complexes, the $Pt–CH_3$ bonds strengthen [14], and the vapor decomposition is presumably accompanied by the detachment of the β-diketonate ligand and pyridine [15]. Since the strength of the Pt–Py bond in the $[(CH_3)_3PtLPy]$ complexes with non-fluorinated β-diketones is lowest [19, 20], their application in MOCVD processes can be accompanied by the degradation of the precursor vapors in the reactor volume. The trimethylplatinum(IV) complexes with tridentate ligands in which the platinum atom coordinates the donor atoms due to the formation of chelate metallocycles are an alternative to the non-fluorinated precursors $[(CH_3)_3PtLPy]$.

The purpose of this work is the refinement of the structure of trimethylplatinum(IV) iodide $[(CH_3)_3PtI]_4$ (**I**) and the synthesis and studies of the structure and thermal properties of complex (*N*,*N*-dimethylaminoethyl)imino-2-penten-3-ol-4-trimethylplatinum(IV) $[(CH_3)_3Pt(C_9H_{17}N_2O)]$ (**II**), which is one of the first representatives of trimethylplatinum(IV) precursors with the tridentate β-iminodiketonate ligand.

Complex **II** was tested in the MOCVD process for the fabrication of Pt films.

## EXPERIMENTAL

The following starting reagents for the synthesis of the trimethylplatinum(IV) complexes were used as received: $K_2PtCl_6$ (Pt 39.82%, Aurat); $CH_3I$ (≥98%, Sigma-Aldrich); *N*,*N*-dimethylethylenediamine (Dmeda, ≥99%, ρ = 0.807 g/mL, Acros Organics); acetylacetone (HAcac, ≥99%, ρ = 1 g/mL, Acros Organics); $I_2$, KOH, and HCl (all analytical grade); $CaSO_4$ (reagent grade); ethanol (96%); acetone (reagent grade); and heptane (analytical grade). A Mg strip (high-purity grade) was mechanically cleaned from magnesium oxides. Diethyl ether (analytical grade) and benzene (reagent grade) were distilled in an inert atmosphere prior to synthesis.

Analyses to C, H, and N were carried out on a CARLO-ERBA-11008 instrument. IR spectra were recorded on a Scimitar FTS 2000 instrument in a range of 400–4000 $cm^{-1}$ (pellets with KBr). Band assignment was performed by comparing with published data [16]. The $^1H$ and $^{13}C$ NMR spectra of solutions of complex **II** in $CDCl_3$ at 25°C were recorded on a Bruker Avance 500 Plus spectrometer. Chemical shifts were determined using the solvent as an internal standard ($^1H$ = 7.26 ppm, $^{13}C$ = 77.7 ppm) [21]. The mass spectrum was detected on a high-resolution mass spectrometer with direct injection (Thermo Scientific Double Focusing Sector) at an accelerating voltage of 70 eV, $T$ = 100°C, and $P = 10^{-7}$ Torr.

**Synthesis of $[(CH_3)_3PtI]_4$ (I)** was carried out in an inert atmosphere using the Schlenk technique according to a published procedure [22]. A Grignard solution was prepared in the Schlenk flask using Mg (1.32 g, 0.055 mol), $CH_3I$ (8 mL, 0.056 mol), and iodine crystals. A Grignard suspension was added dropwise through a funnel to a cooled to –20°C solution of $K_2PtCl_6$ (4.86 g, 0.01 mol) in a mixture of benzene (40 mL) and ether (10 mL). The reaction mixture was heated to room temperature and stirred for 4 h under argon until the mixture turned colorless. The precipitate was filtered off, the mother solution was cooled to 0°C, and ice-cold acetone (5 mL) was added dropwise. The reaction mixture turned yellow-orange with two layers. The flask was opened for air access, ice-cold water (25 mL) was added to the reaction mixture with stirring, and the mixture was acidified with 10% HCl (30 mL). The organic fraction was separated on the funnel, and the aqueous fraction was extracted with 30-mL aliquots of benzene until transparent extracts were obtained. The extracts were combined with the organic fraction and dried over anhydrous $CaSO_4$. The solvent was evaporated to dryness on a rotary evaporator. The yield of white crystals of complex **I** was 2.38 g (65%).

| For $C_{12}H_{36}I_4Pt_4$ | | |
|---|---|---|
| Anal. calcd., % | C, 9.80 | H, 2.45 |
| Found, % | C, 9.69 | H, 2.52 |

**Synthesis of *N*,*N*,*O*-β-iminoketone ($C_9H_{18}N_2O$)** was conducted by the interaction of stoichiometric amounts of Dmeda (8 mL, 0.056 mol) and H(Acac) (5.6 mL, 0.056 mol) in heptane (20 mL) in cold. After 24 h, the organic fraction was collected (the aqueous fraction was formed due to the condensation of the reagents) and fractional distillation was carried out at 130°C thus purifying $C_9H_{18}N_2O$ from residues of the starting reagents. The crystals of $C_9H_{18}N_2O$ were formed in the flask on cooling to 0°C. The yield was 4.75 g (50%).

| For $C_9H_{18}N_2O$ | | | |
|---|---|---|---|
| Anal. calcd., % | C, 63.49 | H, 10.67 | N, 16.45 |
| Found, % | C, 63.63 | H, 10.60 | N, 16.12 |

$^1H$ NMR (500 MHz; δ, ppm): 16.47 (s, O–H), 5.49 (s, C–H), 2.38 (m, 4H, –C**H**$_2$–N$(CH_3)_2$), 2.27 (s, 6H, N$(CH_3)_2$), 2.07 (s, 3H, (N=CC**H**$_3$)), 2.04 (s, 3H, (CO)C**H**$_3$)), 1.97 (m, 4H, C**H**$_2$–$CH_2$–N$(CH_3)_2$).

**Synthesis of $[(CH_3)_3Pt(C_9H_{17}N_2O)]$ (II).** An alcoholic solution (25 mL) of KOH (0.17 g, 0.003 mol) and $C_9H_{18}N_2O$ (0.51 g, 0.003 mol) was added to a solution of $[(CH_3)_3PtI]_4$ (**I**) (1 g, 0.003 mol) in benzene (25 mL). The reaction mixture was stirred in a water bath for 12 h. After solvent evaporation, the dry residue was sublimed at 110°C and $10^{-2}$ Torr, and colorless crystals of complex **II** suitable for XRD study were collected. The yield was 0.92 g (75%).

| For $C_{12}H_{26}N_2OPt$ | | | |
|---|---|---|---|
| Anal. calcd., % | C, 35.20 | H, 6.42 | N, 6.84 |
| Found, % | C, 35.01 | H, 6.60 | N, 6.53 |

IR (KBr; ν, $cm^{-1}$): 3121, 3070, 2954 ν(C–H), 2872 ν(N–$CH_3$), 1580, 1549, 1525, 1500 ν(C=O + C=C), 1445, 1429, 1391 δ(H–C–H), 635–425 ν(Pt–C, Pt–N, Pt–O). $^1H$ NMR (500 MHz; δ, ppm): 0.88 (3H, $J_{Pt-H}$ = 70 Hz, Pt–$CH_3$), 0.96 (6H, $J_{Pt-H}$ = 74 Hz, Pt–$CH_3$), 2.07 (s, 3H, (CN$(CH_3)_2$)C**H**$_3$)), 2.16 (s, 3H, (CO)C**H**$_3$)), 2.27 (s, 6H, N$(CH_3)_2$), 2.51 (tt, 4H, –C**H**$_2$–N$(CH_3)_2$), 3.39 (tt, 4H, C**H**$_2$–$CH_2$–N$(CH_3)_2$), 5.09 (s, C–H). $^{13}C$ NMR (125.76 MHz; δ, ppm): –13.43 ($CH_3$–Pt, $^1J_{C-Pt}$ = 785 Hz), 20.41 ((**C**$H_3$–C(N$CH_3)_2$), 28.41 (**C**$H_3$–C(O), 43.07 (–C**H**$_2$–N$(CH_3)_2$), 44.82 (N$(CH_3)_2$), 56.87 (–C**H**$_2$–C**H**$_2$–N$(CH_3)_2$), 93.12 (**C**H), 164.67 ($CH_3$–**C**(N$(CH_3)_2$)), 191.03 ($CH_3$–**C**O).

**Table 1.** Crystallographic data and structure refinement parameters for compounds **I** and **II**

| Parameter | Value | |
|---|---|---|
| | **I** | **II** |
| Empirical formula | $C_{12}H_{36}I_4Pt_4$ | $C_{12}H_{26}N_2OPt$ |
| *FW* | 1468.37 | 409.44 |
| Space group | $P2_1/c$ | $P\bar{1}$ |
| *a*, Å | 17.2522(8) | 8.0822(2) |
| *b*, Å | 19.3124(10) | 8.4343(3) |
| *c*, Å | 17.6678(10) | 22.8958(6) |
| α, deg | | 90.255(1) |
| β, deg | 116.143(2) | 90.263(1) |
| γ, deg | | 113.619(1) |
| Volume, Å$^3$ | 5284.4(5) | 1429.96(7) |
| *Z* | 8 | 4 |
| $\rho_{calc}$, g/cm$^3$ | 3.691 | 1.902 |
| Range of data collection over θ | From 1.315° to 33.526° | From 0.889° to 33.457° |
| Range of *h*, *k*, *l* | $-26 \le h \le 19$,<br>$-24 \le k \le 29$,<br>$-26 \le l \le 25$ | $-11 \le h \le 12$,<br>$-12 \le k \le 12$,<br>$-35 \le l \le 28$ |
| Number of measured reflections | 67820 | 18560 |
| Number of independent reflections ($R_{int}$) | 18287 (0.0563) | 9172 (0.0282) |
| Completeness of data collection over θ = 25.242°, % | 99.9 | 100.0 |
| Number of reflections/restraints/parameters | 18287/0/385 | 9176/0/318 |
| *S* factor for $F^2$ | 0.964 | 1.109 |
| *R* factor ($I > 2\sigma(I)$) | $R_1 = 0.0426$,<br>$wR_2 = 0.0722$ | $R_1 = 0.0380$,<br>$wR_2 = 0.0680$ |
| *R* factor (all data) | $R_1 = 0.1097$,<br>$wR_2 = 0.0822$ | $R_1 = 0.0476$,<br>$wR_2 = 0.0712$ |

Mass spectrum (70 eV, *m/z* (*I*%)): ($^{195}$Pt) 409(54) $[M]^+$, 365(24) $[M-N(CH_3)_2]^+$, 296(13) $[(CH_3)_3Pt(CH_3COCH)]^+$, 240(100) $[(CH_3)_3Pt]^+$.

**XRD** of the complexes was conducted using a standard procedure on a Bruker-Nonius X8Apex automated four-circle diffractometer equipped with a two-coordinate CCD detector (graphite monochromator, Mo$K_\alpha$ radiation, λ = 0.71073 Å) at *T* = 150 K for complex **II** and at 296 K for complex **I**. Reflection intensities were measured in the φ scan mode of narrow (0.5°) frames. An absorption correction was applied semiempirically using the SADABS program [23]. The structures were solved by a direct method and refined by full-matrix least squares in the anisotropic (for non-hydrogen atoms) approximation using the SHELXTL software [24]. Hydrogen atoms were refined in the rigid body approximation. Experimental structure refinement details for compounds and **I** and **II** are given in Table 1. Selected interatomic distances and bond angles are listed in Table 2.

The crystallographic data for complexes **I** and **II** were deposited with the Cambridge Crystallographic Data Centre (CIF files CCDC nos. 22330007 and 22330008, respectively; deposit@ccdc.cam.ac.uk or www.ccdc.cam.ac.uk/data_reguest/cif).

Quantum chemical calculations were performed in the ADF2022 program complex [25] using the DFT approach combining the Perdew–Burke–Ernzerhof (PBE) functional [26] and the Slater-type all-electron contracted triple zeta valence plus polarization function (TZP/ADF) basis set. Scalar relativistic effects were taken into account at the zero order regular approximation (ZORA) level [27]. The energy of the Pt–ligand bond was calculated for each compound as the difference between the energies of formation (with a correction to the zero point energies) of the optimized structure of the compound and the sum of the energies of formation of the ligands and compounds without ligands (with allowance for the charge). Imag-

**Table 2.** Selected interatomic distances (Å) and angles (deg) for the coordination mode $[(CH_3)_3Pt(C_9H_{17}N_2O)]$ (**II**)

| Bond | *d*, Å | Bond | *d*, Å |
|---|---|---|---|
| Pt(1)–C(11) | 2.035(6) | Pt(2)–C(21) | 2.048(6) |
| Pt(1)–C(12) | 2.025(5) | Pt(2)–C(22) | 2.025(5) |
| Pt(1)–C(13) | 2.048(6) | Pt(2)–C(23) | 2.024(6) |
| Pt(1)–O(1) | 2.128(4) | Pt(2)–O(2) | 2.124(4) |
| Pt(1)–N(11) | 2.105(4) | Pt(2)–N(21) | 2.104(5) |
| Pt(1)–N(12) | 2.230(5) | Pt(2)–N(22) | 2.256(4) |
| Angle | ω, deg | Angle | ω, deg |
| C(12)Pt(1)C(13) | 86.6(3) | C(23)Pt(2)C(22) | 87.1(3) |
| C(12)Pt(1)N(11) | 98.1(2) | C(22)Pt(2)C(21) | 87.3(3) |
| C(13)Pt(1)N(11) | 174.1(2) | C(22)Pt(2)N(21) | 96.6(2) |
| N(11)Pt(1)O(1) | 87.94(16) | C(21)Pt(2)O(2) | 89.3(2) |
| C(11)Pt(1)N(12) | 92.2(2) | C(23)Pt(2)N(22) | 92.4(2) |
| N(11)Pt(1)N(12) | 75.18(17) | C(21)Pt(2)N(22) | 100.2(2) |
| C(12)Pt(1)C(11) | 86.7(3) | O(2)Pt(2)N(22) | 93.43(16) |
| C(11)Pt(1)C(13) | 88.6(3) | C(23)Pt(2)C(21) | 88.4(3) |
| C(11)Pt(1)N(11) | 95.1(2) | C(23)Pt(2)N(21) | 94.9(2) |
| C(12)Pt(1)O(1) | 87.5(2) | C(22)Pt(2)O(2) | 87.3(2) |
| C(13)Pt(1)O(1) | 88.9(2) | N(21)Pt(2)O(2) | 87.72(16) |
| O(1)Pt(1)N(12) | 93.72(16) | N(21)Pt(2)N(22) | 76.01(18) |

inary frequencies are absent from all optimized structures.

Thermogravimetric (TG) analysis of complex **II** was carried out on a Netzsch TG 209 F1 Iris instrument with the enclosed Proteus analysis program package. The sample weight was 10 ± 2 mg. Experiments were carried out in a He atmosphere (30.0 mL/min, $Al_2O_3$ crucible, 10°C/min).

Experiments on the deposition of Pt films from complex **II** on Si(100) plates 1 × 1 $cm^2$ in size were carried out in a flow type MOCVD reactor with cold walls. The process was conducted at the fixed parameters: in an oxidative atmosphere ($\nu(O_2) = 1$ L $h^{-1}$), in a flow of argon as the carrier gas ($\nu(Ar) = 2$ L $h^{-1}$), under a pressure in the reactor of 1 Torr, and at a temperature of the source of 90°C for 60 min. The temperature of film deposition was 280, 310, and 330°C to obtain samples Pt-1, Pt-2, and Pt-3, respectively.

The phase compositions of the samples were determined on a Bruker D8 Advance powder X-ray diffractometer ($CuK_\alpha$ radiation, LYNXEYE XE-T linear detector, 5°–65° 2θ range, 0.03° 2θ increment, acquisition 5 s at point). The size of the coherent scattering region (CSR) was estimated by the Scherrer equation [28]. The morphology of the film surface was studied by scanning electron microscopy (SEM) on a JEOL-ISM 6700 F instrument equipped with an EX-2300BU EDX analyzer for the estimation of the elemental compositions of the films. The sample composition was studied from a surface area of 500 × 400 $\mu m^2$.

## RESULTS AND DISCUSSION

Crystals of the $[(CH_3)_3PtI]_4$ (**I**) phase were isolated from the synthesis of the initial reagent. Only the lattice parameters ($a = 17.77(5)$, $b = 18.99$, $c = 19.39(5)$ Å, $\beta = 115.4(5)°$, $P2_1/a$, $Z = 32$) were presented and the coordinates of the Pt and I (iodine) atoms were determined for $[(CH_3)_3PtI]_4$ (**I**) in [29], whereas the coordinates of light C and H atoms were not determined. Therefore, all structural parameters were completely determined for $[(CH_3)_3PtI]_4$ in our work.

The structure of complex $[(CH_3)_3Pt(C_9H_{17}N_2O)]$ (**II**) contains two crystallographically independent molecules of similar structure. One of the molecules exhibits the orientation disordering of the $-N(CH_3)_2$ group. The coordination sphere around the platinum atoms consists of distorted tetrahedra, whose vertices are occupied by three carbon atoms from the $CH_3$ ligands and the oxygen atom and two nitrogen atoms from iminoketonate (Fig. 1a). The Pt–N distances inside the six-membered metallocycles of molecules of complex **I** are shorter than the Pt–O distances. The longest distances are $Pt–N(CH_3)_2$ (Table 2). The CPtC angles are close and do not exceed 90°. In the five-membered metallocycles of complex **II**, the

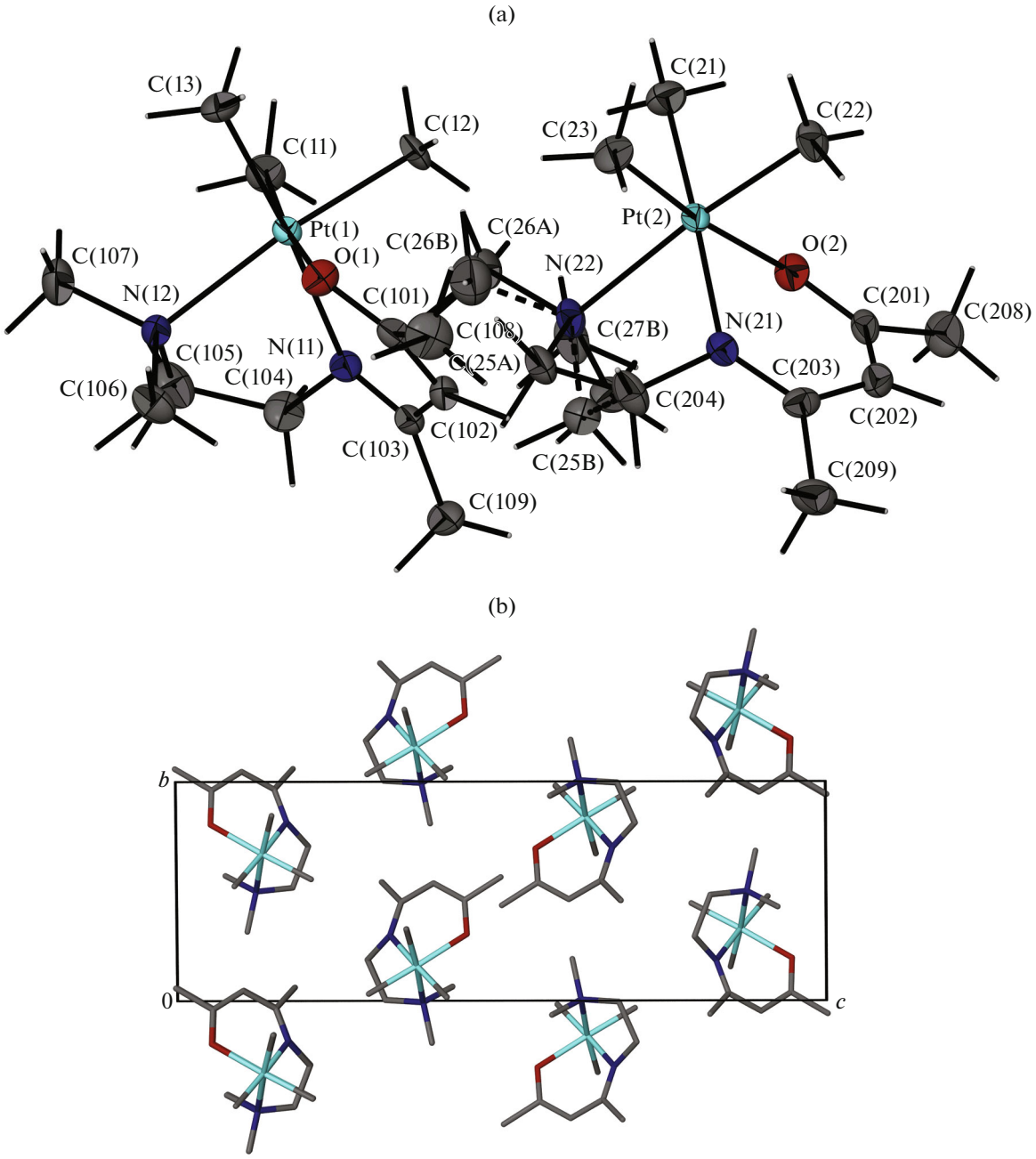


**Fig. 1.** (a) Independent part of the crystal cell of complex **II** with the numeration of atoms in ellipsoid representation (50% probability) and (b) packing along the *a* axis.

NPtN angles (75.18(17)°–76.01(18)°) exhibit the most deviation from 90°.

A comparison with similar in structure complexes of the $[(CH_3)_3Pt(L)Py]$ type (Table 3) revealed that a change in the coordination mode from PtC(3)O(2)N to PtC(3)ON(2) exerted the greatest effect on the Pt–O and Pt–N bond lengths rather than on the Pt–C lengths. The averaged Pt–O distance in the structure of complex **II** is shorter than the average Pt–O distance for $[(CH_3)_3Pt(Acac)Py]$ (**III**), which possibly indicates an enhancement of the strength of platinum binding with the ligand (Table 3). Bent pseudolayers with the hexagonal arrangement of the molecules (Fig. 1b) with the shortest distances between the platinum atoms of the adjacent molecules (6.802 Å) can be distinguished in the packing. Only van der Waals contacts are observed between the molecules. Note that the molecules are packed in layers or chains in the structures of $[(CH_3)_3Pt(R^1COCHCOR^2)Py]$ [17, 19, 20], whereas dimers built on hydrogen bonds are

**Table 3.** Comparison of the main chelate distances (Å) in the series of the trimethylplatinum complexes

| Complex | L = $R^1COCHCOR^2$ | | Pt–C, Å | Pt–O, Å | Pt–N(Py), Å | Literature |
|---|---|---|---|---|---|---|
| | $R^1$ | $R^2$ | | | | |
| $[(CH_3)_3Pt(L)Py]$ | $CF_3$ | $CF_3$ | 2.030(5) | 2.160(8) | 2.181(1) | [17] |
| | $CF_3$ | $CH_3$ | 2.030(9) | 2.155(2) | 2.184(1) | |
| | $CF_3$ | $^t$Bu | 2.029(9) | 2.149(1) | 2.179(1) | [19] |
| | $CF_3$ | $C_4H_3S$ | 2.028(8) | 2.147(3) | 2.170(3) | |
| | $^t$Bu | $C(CH_3)_2OCH_3$ | 2.021(8) | 2.123(1) | 2.159(4) | |
| | $^t$Bu | $^t$Bu | 2.031 | 2.134 | 2.166 | [30] |
| | $CH_3$ | $CH_3$ | 2.036(5) | 2.136(9) | 2.172(1) | |
| | $C_2F_5$ | $CH_3$ | 2.031(8) | 2.152(8) | 2.173(1) | [20] |
| | $C_3F_7$ | $CH_3$ | 2.030(8) | 2.143(3) | 2.162(3) | |
| $[(CH_3)_3Pt(C_9H_{17}N_2O)]$ (**I**) | $CH_3$ | $CH_3$ | 2.033(10) | 2.104(2) | Pt–$N(CH_3)_2$, Å 2.242(5) | This work |

formed in the case of compound **III** ($R^1 = R^2 = CH_3$) [30].

According to the calculation results, the electron density of highest occupied molecular orbitals (HOMO) is mainly localized on the six-membered metallocycle in both complexes (Figs. 2a, 2c). For the lowest unoccupied molecular orbitals (LUMO), the density is localized in different ways: in the case of complex **II**, the density is almost completely localized on the iminoketonate ligand, whereas for compound **III** the density is localized on pyridine (Figs. 2b, 2d).

To evaluate the applicability of complex **II** for MOCVD, its behavior in the condensed and gas phases was studied by thermogravimetry and mass spectrometry. The TG curve for compound **II** (Fig. 3a, line *2*) was recorded under the same conditions as the TG curves of its closest analogs: complexes **III** (Fig. 3a, line *1*) and $[Pt(Acac)_2]$ (Fig. 3a, line *3*). A comparative analysis of the mass loss curves indicates that all complexes have one mass loss step on heating but transit to the gas phase with a residue of 20% for complex **III**, 10% for complex **II**, and 11% for $[Pt(Acac)_2]$. The sublimation of all complexes occurs without significant mass loss. Thus, under the TG experimental conditions, the complexes decompose presumably after melting. One endothermic effect at 106°C corresponding to melting is observed on the DTA curve of studied complex **II** (Fig. 3b). The absence of directed intermolecular contacts in the structure of complex **II** causes its lower melting point ($T_m$ = 106°C, DTA) over that of its closest analog **III** ($T_m$ = 114°C, DSC [14]) but is not accompanied by increasing volatility. The qualitative estimation of the volatility (according to the TG data, at points *T* 50% mass loss) indicates that compound **III** is most volatile compared to complex **II** and both complexes are more volatile than $[Pt(Acac)_2]$.

An analysis of the mass spectrum of complex **II** shows that this compound is monomeric in the gas phase. In the spectrum of complex **II**, the ion with the highest mass is $[(CH_3)_3Pt(C_9H_{17}N_2O)]^+$. The fragmentation of complex **II** proceeds via the cleavage of the $Pt–N(Me)_2$ bond (Pt–N(Py) for **III** according to [15]) followed by the decomposition of the iminoketonate ligand and formation of the most stable metal-containing ion $[(CH_3)_3Pt]^+$. According to the DFT calculations (Table 4), the ionization energy (electron elimination from complex **II**) was estimated as 451 kJ/mol. Note that the ionization of complex **III** is more expended (~510 kJ/mol), whereas that of the Pt–Py bond cleavage is substantially lower: 73.9 kJ/mol (Table 4). Thus, the performed calculations are consistent with the data observed in [17], which explains the absence of the molecular ion peak in the mass spectrum of complex **III**.

The energy of detachment of *N*,*N*,*O*-iminoketonate from complex **I** was calculated using the DFT method (Table 4), since this route was assumed to be one of the most probable ways taking into account the presence of the $[(CH_3)_3Pt]^+$ ion in the spectrum. The energies of detachment of ligands Acac and Py from compound **III** were also calculated for comparison (Table 4). A comparison of the DFT calculation data showed that the detachment of ligands Py and $Acac^-$ or $C_9H_{17}N_2O^-$ is conjugated with significant energy expenses for the molecules of complexes **III** and **II** in the gas phase. The energy necessary for the detachment of ligand $C_9H_{17}N_2O^-$ from complex **I** is insignificantly higher than the energy of the simultaneous

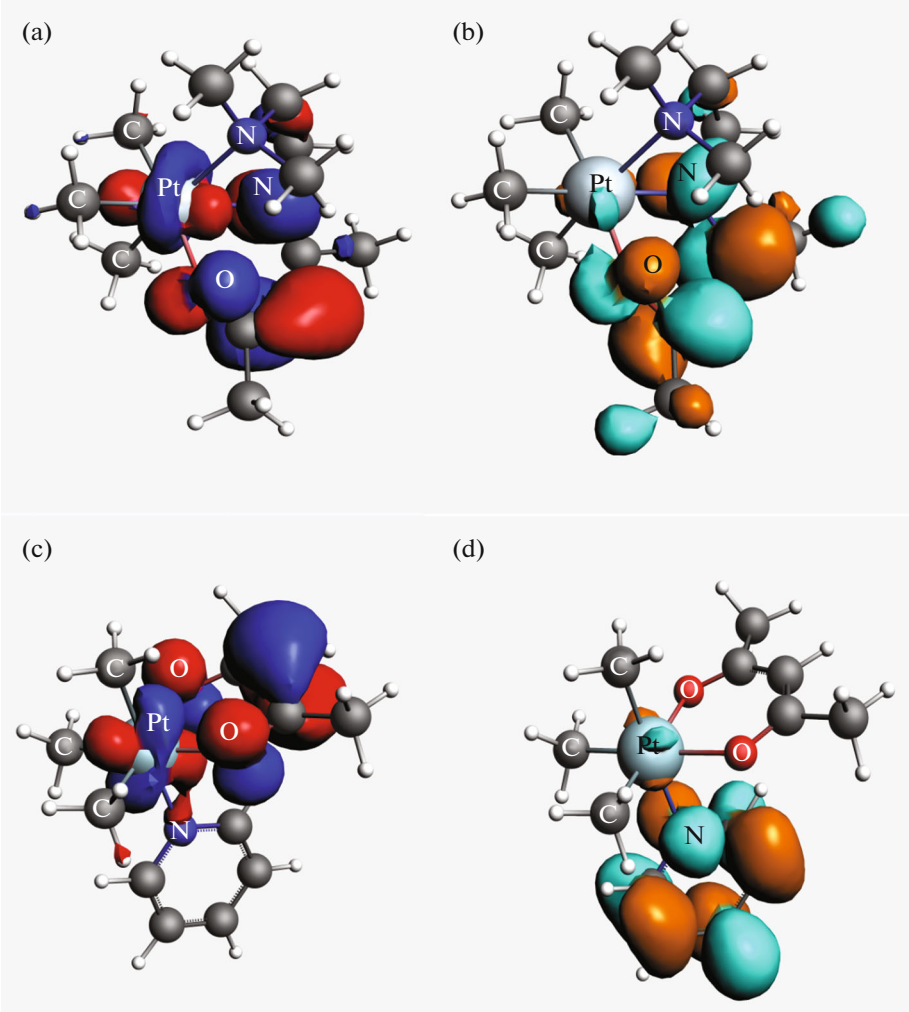


**Fig. 2.** Visualization of the HOMO and LUMO for complexes (a, b) **II** ([$(CH_3)_3Pt(C_9H_{17}N_2O)$]) and (c, d) **III**.

detachment of two ligands (Py and Acac) from compound **III** (Table 4). Since the $[(CH_3)_3Pt(Acac)]^+$ ion is most intense in the mass spectrum of complex **III** [17], it can be expected that the detachment of ligands Py and Acac from the molecule of compound **III** proceeds consequently, and this detachment is less expended in energy in this case. For complex **II**, the detachment of the whole iminoketonate ligand in the gas phase does not presumably occur, and the intramolecular decomposition of the ligand with the formation of the $[(CH_3)_3Pt]^+$ fragment is most probable. Thus, taking into account a stronger binding of Pt with the iminoketonate ligand compared to Pt binding with the β-diketonate analog (XRD data) and the fact that iminoketonate ligand detachment is more expended than the simultaneous detachment of the β-diketonate ligand and pyridine, it can be assumed that vapors of complex **II** in a vacuum are more stable compared with vapors of compound **III**.

**Table 4.** Calculated ionization energies and energies of fragment detachment from complexes $[(CH_3)_3Pt(C_9H_{17}N_2O)]$ (**II**) and $[(CH_3)_3Pt(Acac)Py]$ (**III**)

| Complex | Ionization energy, kJ/mol | Fragment after ligand detachment | Energy of fragment detachment, kJ/mol |
|---|---|---|---|
| **II** | 451 | $[(CH_3)_3Pt]^+$ | 754.3 |
| **III** | 510 | | 753.2 |
| | | $[(CH_3)_3Pt(Acac)]$ | 73.9 |

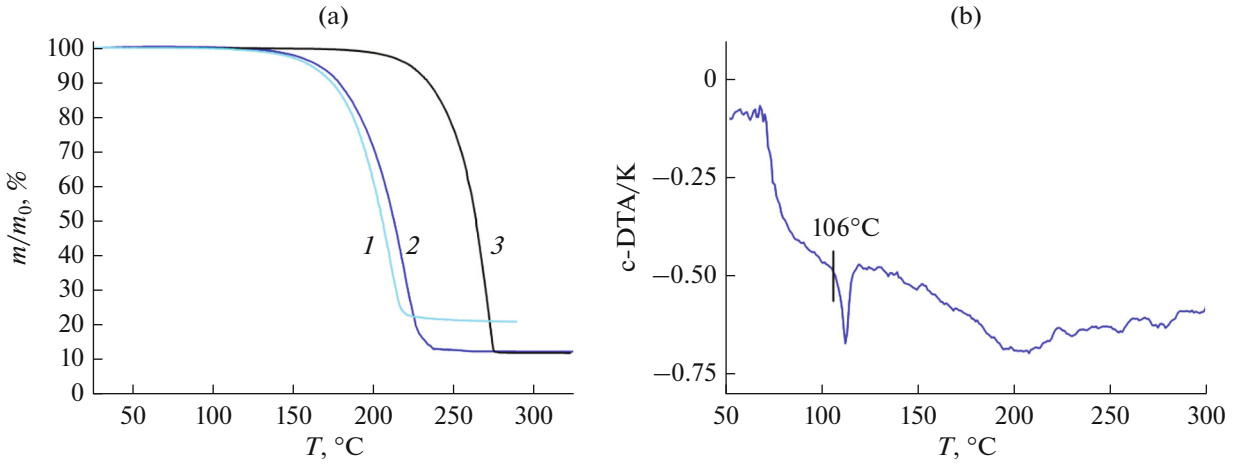


**Fig. 3.** (a) TG curves of complex **II** (line *2*) compared with its analogs **III** (line *1*) and [Pt(Acac)$_2$] (line *3*) and (b) DTA curve of complex **II**.

Complex **II** was tested by the MOCVD method for the first time to fabricate films in an oxygen atmosphere in a temperature range of 280–330°C chosen on the basis of studies on the deposition of the Pt-containing films from compound **III**, [$(CH_3)_3$Pt(Hfac)Py] ($R^1 = R^2 = CF_3$) [15, 20]. The XRD data confirm the formation of Pt films in the whole temperature range (Fig. 4). Remarkably, all formed films (samples Pt-1, Pt-2, Pt-3) have a pronounced (111) texture. Although the growth of fcc metals in the (111) direction is preferable [31], the Pt films with the pronounced texture were earlier prepared from compound **III** only in a hydrogen atmosphere [15]. The Pt films without pronounced orientation were fabricated from both complexes [$(CH_3)_3$Pt(Acac)Py] and [$(CH_3)_3$Pt(Hfac)Py] in an oxidative atmosphere [15, 20]. The formation of (111)Pt films on the Si plate was reported [32], but the [$(CH_3)_3$Pt($Cp^{Me}$)] precursor and higher deposition temperatures (350°C) were used in this case. Nearly all samples have narrow (111) reflections, which makes it possible to estimate their CSR (only roughly) as >100 nm. According to the EDX data, the samples contain Pt in an amount of 85–88 at %, as well as C (9–11 at % content) and O (3–4 at % content). According to the SEM data, the surface of the Pt-1 sample is smooth and formed by particles ~100 nm in size (Fig. 5a). An increase in the deposition temperature leads to particle confluence (Fig. 5b, sample Pt-2) or the formation of clusters from the particles (Fig. 5c, sample Pt-3). The study of the transversal cross section of the samples indicates an increase in their thicknesses from 80 to 170 nm with increasing deposition temperature from 280 to 330°C, respectively. The samples have the column structure (Figs. 5d–5f) typical of the Pt films fabricated by the MOCVD method.

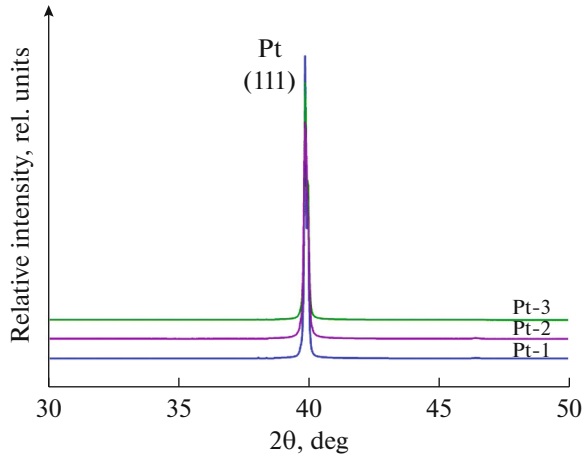


**Fig. 4.** XRD patterns of the film samples derived from complex **II**.

To conclude, molecules of the complexes in the crystals of [$(CH_3)_3$Pt($C_9H_{17}N_2O$)] (**II**) have a pseudolayer packing, and only van der Waals contacts are observed between the molecules. The crystal structure of [$(CH_3)_3$PtI]$_4$ was refined. A comparative analysis of the thermal properties of complex **II** and its analogs showed that a change in the coordination mode from $PtC_3O_2N$ ([$(CH_3)_3$Pt(Acac)]Py) to $PtC_3ON_2$ [$(CH_3)_3$Pt($C_9H_{17}N_2O$)] enhances the thermal stability of complex **II** in the condensed state, but the volatility does not increase. The probable mechanism of fragmentation of complex **II** with the formation of the most stable fragment $[(CH_3)_3Pt]^+$ was proposed using the quantum-chemical calculations and mass spectrometry data. The Pt films with the pronounced (111) texture were obtained on the Si(100) substrates by the MOCVD method using complex **II** as a precursor in a temperature range of 280–330°C in an oxidative atmosphere.

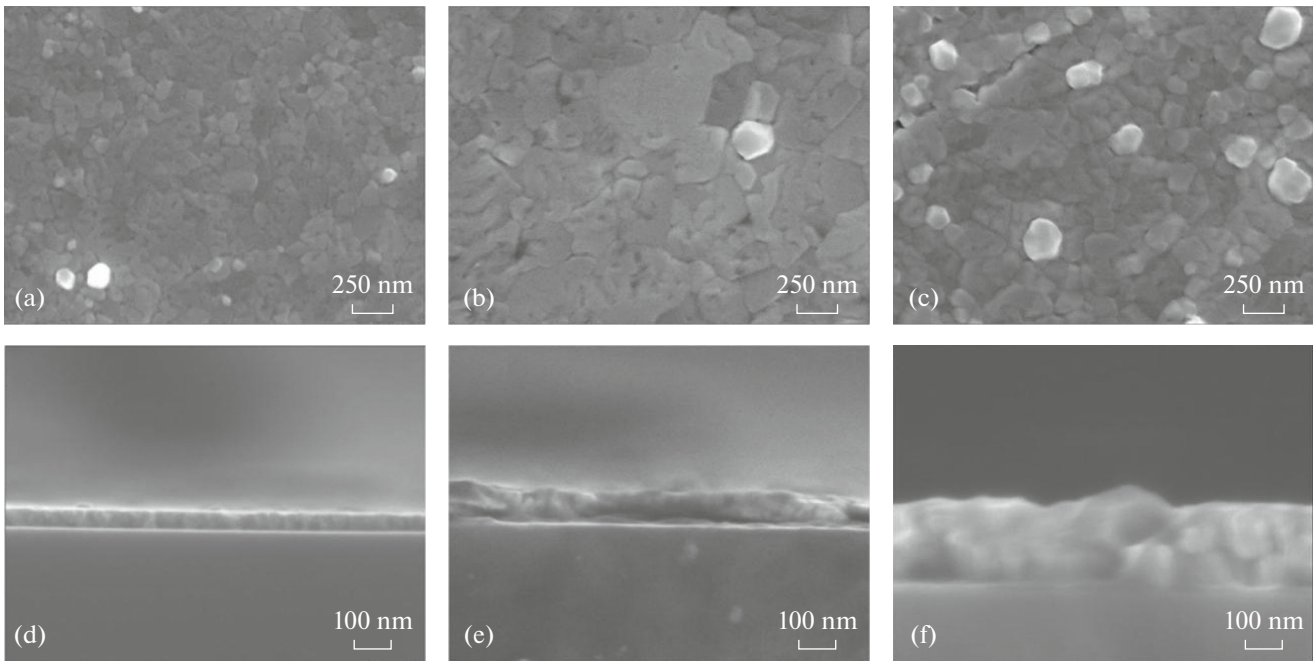


**Fig. 5.** SEM images of the surface of the (a) Pt-1, (b) Pt-2, and (c) Pt-3 films and cross sections of (d) Pt-1, (e) Pt-2, and (f) Pt-3.

## ACKNOWLEDGMENTS

The authors are grateful to E.S. Vikulov, I.V. Mirzaev, and D.A. Piryazev.

## FUNDING

This work was supported by the Ministry of Science and Higher Education of the Russian Federation, projects nos. 121031700313-8 and 121031700314-5.

## CONFLICT OF INTEREST

The authors of this work declare that they have no conflicts of interest.

## REFERENCES

1. Liang, L.C., Liao, S.M., and Zou, X.R., *Inorg. Chem.*, 2021, vol. 60, no. 20, p. 15118. https://doi.org/10.1021/acs.inorgchem.1c02494
2. Skabitsky, I.V., Romadina, E.I., Sakharov, S.G., et al., *J. Organomet. Chem.*, 2019, vol. 896, p. 77. https://doi.org/10.1016/j.jorganchem.2019.05.008
3. Lien, C., Sun, H., Qin, X., et al., *Surf. Sci.*, 2018, vol. 677, p. 161. https://doi.org/10.1016/j.susc.2018.07.002
4. Thurier, C. and Doppelt, P., *Coord. Chem. Rev.*, 2008, vol. 252, nos. 1–2, p. 155. https://doi.org/10.1016/j.ccr.2007.04.005
5. Komiya, S., Ezumi, S., Komine, N., et al., *Organometallics*, 2009, vol. 28, no. 13, p. 3608. https://doi.org/10.1021/om900319a
6. Pichaandi, K.R., Kabalan, L., Amini, H., et al., *Inorg. Chem.*, 2017, vol. 56, no. 4, p. 2145. https://doi.org/10.1021/acs.inorgchem.6b02801
7. Ghosh, B.N., Lentz, D., Schlecht, S., et al., *New J. Chem.*, 2015, vol. 39, p. 3536. https://doi.org/10.1039/C4NJ02426E
8. Ghosh, B.N., Hausmann, H., Schlecht, S., et al., *ZAAC*, 2013, vol. 639, nos. 12–13, p. 2202. https://doi.org/10.1002/zaac.201300277
9. Ghosh, B.N., Schlecht, S., and Bauzá, A., *New J. Chem.*, 2017, vol. 41, p. 3498. https://doi.org/10.1039/C7NJ00337D
10. Lindner, R., Wagner, C., and Steinborn, D., *J. Am. Chem. Soc.*, 2009, vol. 131, no. 25, p. 8861. https://doi.org/10.1021/ja901264t
11. Lanci, M.P., Remy, M.S., Lao, D.B., et al., *Organometallics*, 2011, vol. 30, no. 14, p. 370. https://doi.org/10.1021/om200508k
12. Baker, L., Cavanagh, A.S., Seghete, D., et al., *ACS Nano*, 2013, vol. 7, no. 7, p. 6337. https://doi.org/10.1021/nn402385f
13. Aaltonen, T., Rahtu, A., and Ritala, M., *Electrochem. Solid-State Lett.*, 2003, vol. 6, no. 9, p. 130. https://doi.org/10.1149/1.1595312
14. Karakovskaya, K.I., Dorovskikh, S.I., Vikulova, E.S., et al., *Coatings*, 2021, vol. 11, no. 1, p. 78. https://doi.org/10.3390/coatings11010078
15. Dorovskikh, S.I., Zharkova, G.I., Turgambaeva, A.E., et al., *Appl. Organomet. Chem.*, 2017, vol. 31, no. 7. e3654. https://doi.org/10.1002/aoc.3654
16. Zharkova, G.I., Baidina, I., Turgambaeva, A., et al., *Polyhedron*, 2012, vol. 40, p. 40. https://doi.org/10.1016/j.poly.2012.03.045

17. Zharkova, G.I., Baidina, I.A., Igumenov, I.K., et al., *Russ. J. Coord. Chem.*, 2011, vol. 37, p. 680. https://doi.org/10.1134/S1070328411080136
18. Mohlala, L.M., Jen, T.-C., and Olubambi, P.A., *Procedia Manuf.*, 2019, vol. 35, p. 1250. https://doi.org/10.1016/j.promfg.2019.06.083
19. Dorovskikh, S.I., Krisyuk, V.V., Mirzaeva, I.V., et al., *Polyhedron*, 2020, vol. 182, p. 114475. https://doi.org/10.1016/j.poly.2020.114475
20. Dorovskikh, S.I., Klyamer, D.D., Mirzaeva, I.V., et al., *J. Fluorine Chem.*, 2021, vol. 249, p. 109843. https://doi.org/10.1016/j.jfluchem.2021.109843
21. Fulmer, G.R., Miller, AJ.M., Sherden, N.H., et al., *J. Organomet.*, 2010, vol. 29, p. 2176. https://doi.org/10.1021/om100106e
22. Baldwin, J.C. and Kaska, W.C., *Inorg. Chem.*, 1975, vol. 14, no. 8, p. 2020. https://doi.org/10.1021/ic50150a063
23. *APEX2 (version 1.08), SAINT (version 7.03), SADABS (version 2.11), SHELXTL (version 6.12)*, Madison: Bruker AXS Inc., 2004.
24. Sheldrick, G., *Acta Crystallogr., Sect. C: Struct. Chem.*, 2015, vol. 71, p. 3. https://doi.org/10.1107/S2053229614024218
25. *ADF 2022. SCM. Theoretical Chemistry*, Amsterdam: Vrije Universiteit, 2022. http://www.scm.com.
26. Lenthe, E., Ehlers, A., and Baerends, E.J., *J. Chem. Phys.*, 1999, vol. 110, no. 18, p. 8943. https://doi.org/10.1063/1.478813
27. Pye, C.C. and Ziegler, T., *Theor. Chem. Acc*, 1999, vol. 101, no. 6, p. 396. https://doi.org/10.1007/s002140050457
28. Kraus, W. and Nolze, G., *J. Appl. Crystallogr.*, 1996, vol. 9, p. 301. https://doi.org/10.1107/S0021889895014920
29. Donnay, G., Coleman, L.B., Krueghoff, N.G., et al., *Acta Crystallogr., Sect. B: Struct. Crystallogr. Cryst. Chem.*, 1968, vol. 24, p. 157.
30. Zharkova, G.I., Baidina, I.A., Naumov, D.Y., et al., *J. Struct. Chem.*, 2011, vol. 52, no. 4, p. 550. https://doi.org/10.1134/S0022476611030152
31. Paul, H., *Adv. Eng. Mater.*, 2010, vol. 12, p. 1029. https://doi.org/10.1002/adem.201000078
32. Goswami, J., Wang, C.-G., Cao, W., and Dey, S.K., *Chem. Vap. Depos.*, 2003, vol. 9, no. 4, p. 213. https://doi.org/10.1002/cvde.20030624033

*Translated by E. Yablonskaya*